Sensors and Actuators B 158 (2011) 333–339

Contents lists available at ScienceDirect

Sensors and Actuators B: Chemical

journal homepage: www.elsevier.com/locate/snb

Analyte selective response in solution-deposited tetrabenzoporphyrin thin-film field-effect transistor sensors

James E. Royer[a], Sangyeob Lee[a], Charlene Chen[b], Byungmin Ahn[c], William C. Trogler[a], Jerzy Kanicki[b,d], Andrew C. Kummel[a,*]

[a] Department of Chemistry and Biochemistry, University of California, San Diego, La Jolla, CA 92093, USA
[b] Department of Electrical Engineering and Computer Science, The University of Michigan, Ann Arbor, MI 48109, USA
[c] Department of Chemical Engineering and Materials Science, University of Southern California, Los Angeles, CA 90089, USA
[d] California Institute for Telecommunications and Information Technology, University of California, San Diego, La Jolla, CA 92093, USA

ARTICLE INFO

Article history:
Received 22 March 2011
Received in revised form 27 May 2011
Accepted 7 June 2011
Available online 14 June 2011

Keywords:
Thin film transistor
Field-effect transistor
Chemical sensor
Semiconductor
Phthalocyanine
Porphyrin
Tetrabenzoporphyrin
Grain size
Adsorption
Lewis-bases
Thin-films
Solution-processed
Morphology

ABSTRACT

Organic thin film transistor (OTFT) chemical sensors rely on the specific electronic structure of the organic semiconductor (OSC) film for determining sensor stability and response to analytes. The delocalized electronic structure is influenced not only by the OSC molecular structure, but also the solid state packing and film morphology. Phthalocyanine (H_2Pc) and tetrabenzoporphyrin (H_2TBP) have similar molecular structures but different film microstructures when H_2Pc is vacuum deposited and H_2TBP is solution deposited. The difference in electronic structures is evidenced by the different mobilities of H_2TBP and H_2Pc OTFTs. H_2Pc has a maximum mobility of 8.6×10^{-4} $cm^2\ V^{-1}\ s^{-1}$ when the substrate is held at 250 °C during deposition and a mobility of 4.8×10^{-5} $cm^2\ V^{-1}\ s^{-1}$ when the substrate is held at 25 °C during deposition. Solution deposited H_2TBP films have a mobility of 5.3×10^{-3} $cm^2\ V^{-1}\ s^{-1}$, which is consistent with better long-range order and intermolecular coupling within the H_2TBP films compared to the H_2Pc films. Solution deposited H_2TBP also exhibits a textured film morphology with large grains and an RMS roughness 3–5 times larger than H_2Pc films with similar thicknesses. Despite these differences, OTFT sensors fabricated from H_2TBP and H_2Pc exhibit nearly identical analyte sensitivity and analyte response kinetics. The results suggest that while the interactions between molecules in the solid state determine conductivity, localized interactions between the analyte and the molecular binding site dominate analyte binding and determine sensor response.

1. Introduction

Organic thin film transistors (OTFTs) have attracted interest as chemical sensing platforms for vapor and liquid phase detection of explosives, toxins and biochemicals [1–7]. OTFTs offer numerous advantages over inorganic oxide and polymer chemiresistors, such as tailored chemical selectivity, room temperature operation, and multiparameter response [8–12]. Several reports demonstrate novel device structures using inexpensive, robust materials providing a low cost fabrication pathway for selective, single use sensing applications [13–15]. However, the organic semiconductor layer is often deposited by vacuum evaporation in order to control film thickness and microstructure, which are key parameters governing sensitivity and stability [16–19]. A potential advantage of organic materials is the possibility of fabricating solution processed sensors using low cost, high throughput deposition methods, such as ink-jet printing and spin-coating. However, for practical devices, the high sensitivity and mobility of vacuum deposited sensors must be retained with solution processing methods.

Porphyrins (Por) and phthalocyanines (Pcs) are a well studied group of sensor materials, characterized by their good thermal stability, high optical absorbance and functionality [20–23]. Porphyrins are structurally related to phthalocyanines, with the four –CH groups in the inner porphyrin ring replacing the four meso nitrogens of phthalocyanine. Several studies have investigated differential chemical sensing by changing the central metal atom in the Por/Pc core or by changing the peripheral substituents [24–27]. Sensing mechanism studies for metal-free phthalocyanine (H_2Pc) thin-films have correlated sensor response with a selective molecular chemisorption event, determined by the hydrogen bond basicity of the analyte [28,29]. The present work expands on the selective

* Corresponding author. Tel.: +1 858 534 3498; fax: +1 858 534 2063.
E-mail address: akummel@ucsd.edu (A.C. Kummel).

0925-4005/$ – see front matter © 2011 Elsevier B.V. All rights reserved.
doi:10.1016/j.snb.2011.06.030

response mechanism of H_2Pc thin-film sensors by demonstrating nearly identical sensor response for H_2Pc and H_2TBP OTFTs with dramatically different film morphologies and bulk electronic structures.

The film morphology and bulk electronic structures of H_2Pc and H_2TBP films were modified using different deposition methods. H_2TBP is deposited with the use of a soluble precursor and thermally converted to form a textured polycrystalline film with large grains and large surface roughness. H_2Pc is deposited by vacuum evaporation while holding the substrate at different temperatures which allows growth of films with significantly different grain size and surface roughness. In general, for H_2Pc at higher substrate deposition temperatures (T_{sub}), there is increased ordering leading to larger grains and increased mobility [30]. Similar correlations between mobility and grain size have been noted for spin-coated H_2TBP films; however the mobilities are often higher than vacuum evaporated H_2Pc films which suggests better intermolecular coupling and long-range order within the grains [31,32]. The present study shows that solution processed H_2TBP and vacuum deposited H_2Pc OTFTs exhibit nearly identical analyte sensitivity and analyte response kinetics despite large differences in the film morphology and bulk electronic structure. The H_2TBP OTFTs have greater than 3× larger RMS roughness, greater than 3× larger grain size and greater than 100× higher mobility than room temperature vacuum deposited H_2Pc OTFTs; yet the analyte sensitivities are equal to within a factor of two for most analytes. The results suggest that sensing properties are determined by selective molecular chemisorption via hydrogen-bonding at the binding site and have little dependence on film microstructure.

2. Materials and methods

H_2TBP and H_2Pc TFT sensors were fabricated using an inverted bottom contact device geometry using a modified bilayer resist lift-off method [33,34]. Briefly, resist layers of PMGI SF8 (Microchem) and S1818 (Shipley) are employed to create an undercut resist profile so that metal deposition yields a tapered electrode geometry. Electrodes consisted of a 5 nm Ti adhesion layer followed by 45 nm of Au deposited under high vacuum on 100 nm thermally grown $SiO_2/n^{++}Si$ (1 0 0) substrates (Silicon Quest). The soluble H_2TBP precursor 1,4:8,11:15,18-22,25-tetraethano-29H,31H-tetrabenzo[b, g, l, q]porphine (CP) was spin-coated in air from a 0.7 wt% chloroform solution and annealed at 200 °C in a N_2 purged oven. Prior to spin coating, the substrates were rinsed in acetone and isopropanol, treated with UV-ozone for 20 min, and soaked in ethanol. Synthesis of CP followed the literature procedure [35]. H_2Pc was purchased from Sigma–Aldrich and purified 3 times by multiple zone sublimation before loading into the deposition chamber. Prior to H_2Pc deposition, the substrates were sonicated in isopropanol and in deionized water. H_2Pc was thermally evaporated in ultra-high vacuum at rates of 0.9–1.0 Å s^{-1} onto rotating substrates held at constant substrate temperature. An H_2Pc film thickness of 100 nm was chosen, which is similar to the estimated thickness of the H_2TBP film [36].

Current–voltage measurements were recorded in air in the dark, immediately following removal from a vacuum storage chamber, using an Agilent B1500 semiconductor parameter analyzer. The mobility and threshold voltage were calculated based on the equation for TFT saturation mode operation, $I_d = (WC_i/2L)\mu_{FE}(V_{gs} - V_{th})^2$ where C_i is the gate oxide capacitance μ_{FE} is the field-effect mobility, V_{th} is the threshold voltage, W is the channel width and L is the channel length. Before chemical sensing, the samples were wire bonded on a ceramic DIP and mounted on a printed circuit board. In order to minimize the effect of device aging, the devices were stored in a chemical free vacuum desiccator for one day prior to chemical sensing.

Table 1
H_2TBP and H_2Pc device properties. Calculated mobility (μ_{FE}), threshold voltage (V_{th}) and I_{on}/I_{off} parameters for vacuum evaporated H_2Pc at different substrate temperatures (T_{sub}) and solution deposited H_2TBP.

T_{sub} (°C)	μ_{FE} ($\times 10^{-4}$ cm^2 V^{-1} s^{-1})	V_{th} (V)	I_{on}/I_{off}
25	0.30 ± 0.08	−4.1 ± 0.4	(2.3 ± 0.4) × 10^3
80	1.57 ± 0.04	−3.3 ± 0.1	(6.4 ± 0.4) × 10^3
125	5.50 ± 0.43	−4.0 ± 0.5	(2.5 ± 1.2) × 10^4
200	5.76 ± 0.07	−4.9 ± 0.4	(2.0 ± 0.1) × 10^4
250	8.37 ± 1.30	−5.1 ± 0.5	(4.2 ± 0.9) × 10^4
Spin-coated H_2TBP	53.7 ± 9.9	−2.9 ± 0.4	(3.7 ± 1.5) × 10^5

AFM measurements were performed with a Nanoscope IV scanning microscope in tapping mode using a Nanosensors SSS-NCHR-20 ultra-sharp Si probe. SEM measurements were performed on a field emission SEM, JSM-2007 from JEOL.

Sensing experiments were performed under zero grade air (Praxair, <2 ppm H_2O, <0.02 ppm NO_x) at 25 °C. A 2% duty cycle pulse train operated at 0.02 Hz was applied for both the gate and drain bias. Transient measurements were recorded using a National Instruments 6211-DAQ by recording the voltage drop across a 1.2 kΩ resistor. Prior to sensing measurements, the devices were operated under zero grade air using the gate pulse sequence to equilibrate the bias stress effect. Analyte vapors were introduced to an enclosed, thermally regulated chamber with electrical feedthroughs by bubbling zero grade air through the liquid analyte. The concentration of analyte introduced was controlled by mixing the saturated vapor with a separate dilution line in a manifold prior to the chamber.

Recovery analysis was performed by comparing t_{60} values, where t_{60} is defined as the time required to recover 60% of sensor response with respect to the baseline current. The t_{60} values were calculated following subtraction of residual baseline current drift. The drift was fit to a linear regression and subtracted from the raw signal to prevent drift from skewing the t_{60} values.

3. Results and discussion

To determine appropriate test parameters for sensor operation, TFTs based on H_2Pc and H_2TBP were electrically characterized. Fig. 1 shows typical current–voltage (I–V) characteristics of H_2Pc (T_{sub} = 25 °C) and solution processed H_2TBP TFTs, with the molecular structures of H_2Pc and H_2TBP as insets in Fig. 1b and d. The mobilities and threshold voltages range from $(3.0 \pm 0.8) \times 10^{-5}$ cm^2 V^{-1} s^{-1} and -4.1 ± 0.4 V for H_2Pc to $(5.3 \pm 0.9) \times 10^{-3}$ cm^2 V^{-1} s^{-1} and -2.9 ± 0.4 V for H_2TBP, which is comparable to previously reported H_2Pc and H_2TBP OTFTs [30,36]. The mobilities, threshold voltages and I_{on}/I_{off} ratios for H_2Pc OTFTs with different T_{sub}, and spin-coated H_2TBP OTFTs are summarized in Table 1. The non-linear behavior of the drain current at low drain voltage in Fig. 1c is consistent with significant source/drain contact resistance and could be attributed to poor step coverage of the H_2TBP at the Au/H_2TBP channel edge [37]. Vapor deposited H_2Pc devices exhibit slightly better contact resistance, as evidenced by the distinct linear region in Fig. 1a, possibly due to enhanced film coverage at the contact interface. Torsi et al. demonstrated that contact resistance cannot be neglected during chemical sensing when the device is operated at low bias conditions [38]. In this work, the devices are operated at sufficiently high drain voltage (V_{ds} = −10 V) and gate voltage (V_{gs} = −8 V) that differences in contact resistance will not affect the sensing properties.

Stable operating conditions for OTFT sensors require careful control of both electrical and environmental test parameters. Stable operation was achieved using dry synthetic air flow and a pulsed gate bias with a 2% duty cycle. The pulsed gate method has been demonstrated as an effective operating method to reduce bias

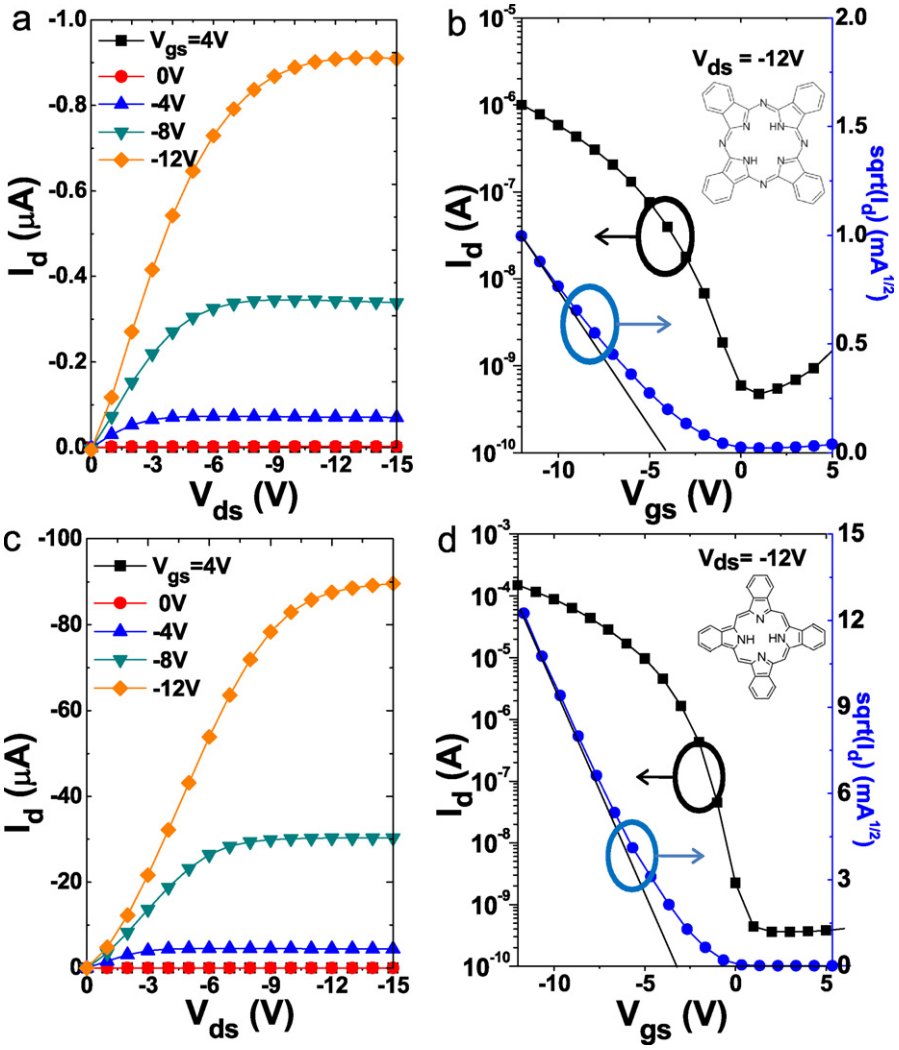

Fig. 1. H_2Pc and H_2TBP OTFT characteristics. Output characteristics of (a) 100 nm vacuum deposited H_2Pc with T_{sub} = 25 °C and (c) solution processed H_2TBP OTFTs. Transfer characteristics of the same (b) H_2Pc and (d) H_2TBP OTFTs. The solid lines indicate fits used to extract threshold voltage and mobility. Gate oxide capacitance (C_i) = 3.45 × 10^{-8} F/cm^2, channel length (L) = 5 μm, channel width (W) = 10^5 μm for both devices, V_{gs} sweep using −1 V steps for (b) and (d).

stress effects for both polymer and small molecule OTFTs [39,40]. By reducing the gate "on" time via pulsing, it is possible to minimize bias induced shifts in threshold voltage during chemical sensing. Following stabilization, the H_2TBP and H_2Pc devices were operated with current drift as low as 0.1% per hour.

Fig. 2 shows the H_2TBP, H_2Pc (T_{sub} = 25 °C) and H_2Pc (T_{sub} = 250 °C) sensor responses to acetonitrile (Fig. 2a) and dimethyl methylphosphonate (Fig. 2b) when operated in the saturation region (V_{ds} = −10 V, V_{gs} = −8 V) using a pulsed gate bias with a 2% duty cycle. The drain currents (I_d) for both devices are normalized and plotted with respect to the initial currents (I_o). The stable baseline allows a well defined response ($\Delta I/I_{baseline} \times 100$), where ΔI is defined by the current change over a 20 min dose period and $I_{baseline}$ is the drain current measured immediately before analyte doses (see Supplementary Data). Five analytes were tested to assess a range of sensor binding affinities where trimethylphosphate (TMP), isophorone (ISO) and dimethyl methylphosphonate (DMMP) are considered strong binders and acetonitrile (ACN) and methanol (MeOH) are considered weak binders [28]. Sensor response was linear with dose concentration, and drain current decreases were observed for all analytes tested. Sensor response for MeOH, TMP and ISO doses can be found in the Supplementary Data (Figs. S1–S3). The sensitivities (% ppm^{-1}) for each analyte are plotted in Fig. 2c, where sensitivity is defined by the slope of the linear fit of the sensor responses versus analyte concentrations (Figs. S4 and S5). For H_2TBP, the sensitivity (S) was greatest for DMMP and lowest for MeOH, with a response ratio (S_{DMMP}/S_{MeOH}) of ~85. The corresponding response ratios for H_2Pc (T_{sub} = 250 °C) and H_2Pc (T_{sub} = 25 °C) were ~53 and ~32. For all sensors, the response ratios between DMMP and weak binding analytes exceeded 30 (Table 2). The high response ratio makes H_2TBP suitable for use in cross-reactive sensor arrays where discriminatory analysis can be used to identify analytes [29]. Although some of the response ratios differ by more than 2× between the H_2Pc and H_2TBP sensors, the relative analyte sensitivities (S_{H_2TBP}/S_{H_2Pc}) differ by less than 2× for all analytes (Tables S1 and S2). This suggests that molecular chemisorption between the analyte and the semiconductor dominates sensor response even though morphological effects may provide slightly enhanced analyte discrimination for H_2TBP.

By analyzing the transient recovery in OTFT chemical sensors, the analyte binding kinetics can be elucidated. Average t_{60} values for each sensor are presented in Table 2. The t_{60} values are normalized with respect to MeOH to illustrate the consistent relative recovery times for each sensor. The relative recovery time normalizes the t_{60} for each recovery with respect to the t_{60} for MeOH. This eliminates run-to-run variations in flow rate or temperature which could influence recovery rates. Both H_2Pc and H_2TBP sensors

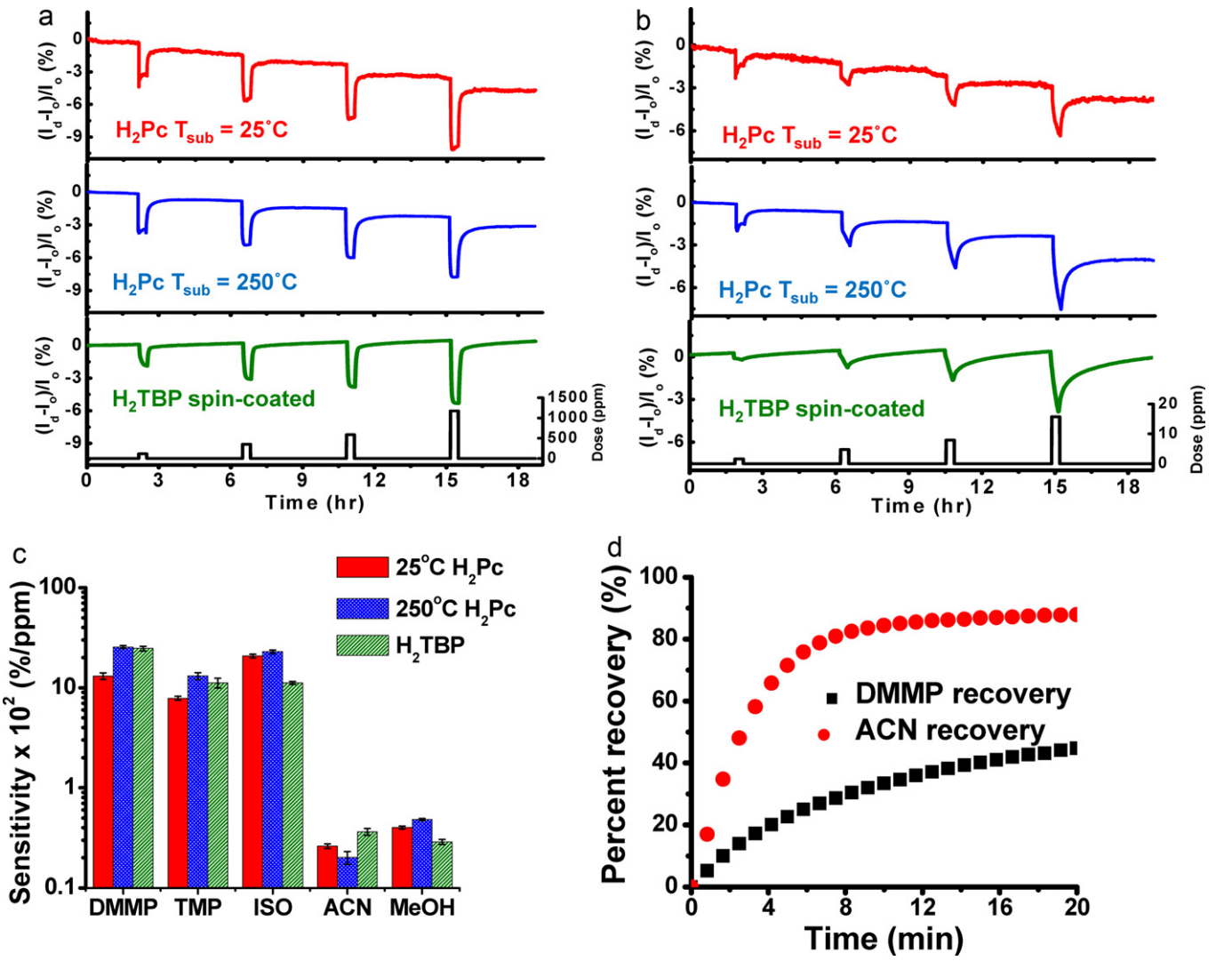

Fig. 2. H_2TBP and H_2Pc OTFT sensing. Transient response of H_2Pc (T_{sub} = 25 °C and 250 °C) and H_2TBP OTFTs to (a) acetonitrile (ACN) and (b) dimethyl methylphosphonate (DMMP). (c) Calculated sensitivities for H_2TBP, and H_2Pc OTFT sensors. Calculations are based on the slope of the linear fit of the sensor responses versus analyte concentration, averaged for three devices. (d) Recovery of H_2TBP sensors following exposure to 1174 ppm ACN and 15.8 ppm DMMP.

exhibit rapid recovery following doses of weak binding analytes such as MeOH and ACN (Fig. 2a), whereas for strong binding analytes such as TMP and DMMP there is a slower recovery (Fig. 2b). The H_2TBP sensor recovery immediately following a 15.8 ppm DMMP exposure and a 1174 ppm ACN exposure is presented in Fig. 2d to illustrate the extended recovery time required for DMMP.

Table 2
Relative recoveries and response ratios for H_2TBP and H_2Pc OTFT sensors. Normalized average t_{60} values for H_2TBP and H_2Pc OTFT sensors following exposure to 400 ppm methanol (MeOH), 587 ppm acetonitrile (ACN), 8.9 ppm isophorone (ISO), 6.2 ppm trimethylphosphate (TMP) and 7.9 ppm dimethyl methylphosphonate (DMMP). The data for each sensor are averaged for three separate devices and normalized with respect to the average t_{60} for MeOH recovery. The standard deviations for each quantity are shown in the parentheses. The response ratios (defined in text) for DMMP to MeOH and for DMMP to ACN for each sensor are listed in the bottom two rows.

	Spin-coated H_2TBP	H_2Pc (T_{sub} = 25 °C)	H_2Pc (T_{sub} = 250 °C)
DMMP	4.8 (0.3)	4.0 (1.1)	4.4 (0.1)
TMP	2.6 (0.1)	1.8 (0.2)	2.9 (0.3)
ISO	2.2 (0.6)	0.7 (<0.1)	0.8 (0.1)
ACN	0.3 (<0.1)	0.7 (<0.1)	0.9 (0.1)
MeOH	1.0	1.0	1.0
S_{DMMP}/S_{MeOH}	85	32	53
S_{DMMP}/S_{ACN}	68	50	126

The results for H_2TBP and H_2Pc OTFTs are analogous to those for previously reported H_2Pc thin-film chemiresistors [28]. The analyte sensing mechanism is attributed to hydrogen-bonding at the inner N_4H_2 group. OTFT on-current decreases are observed during exposure to hydrogen bond acceptor analytes due to electron density donation from the analyte to the interior N–H protons in H_2TBP and H_2Pc. Therefore, analytes which are better hydrogen-bond acceptors such as DMMP and TMP are also stronger Lewis bases [41]. The sensitivities and relative recovery times for H_2TBP and H_2Pc OTFT sensors correlate with the analyte hydrogen-bond basicity.

The distinction in response between strong and weak binding analytes is consistent with a selective molecular chemisorption event between the analyte and semiconductor. Molecular chemisorption between the analyte and semiconductor is due to electron density transfer upon hydrogen-bonding. The magnitude of electron density transfer and binding energy (E_{bind}) distinguishes weak binding analytes as physisorbates (E_{bind} < 0.3 eV) and strong binding analytes as chemisorbates (E_{bind} ~ 1 eV) [42]. The distinction between chemisorbing and physisorbing analytes on H_2TBP and H_2Pc OTFTs is evident not only by the high sensitivities noted above, but also by the relative recovery times. Although taken

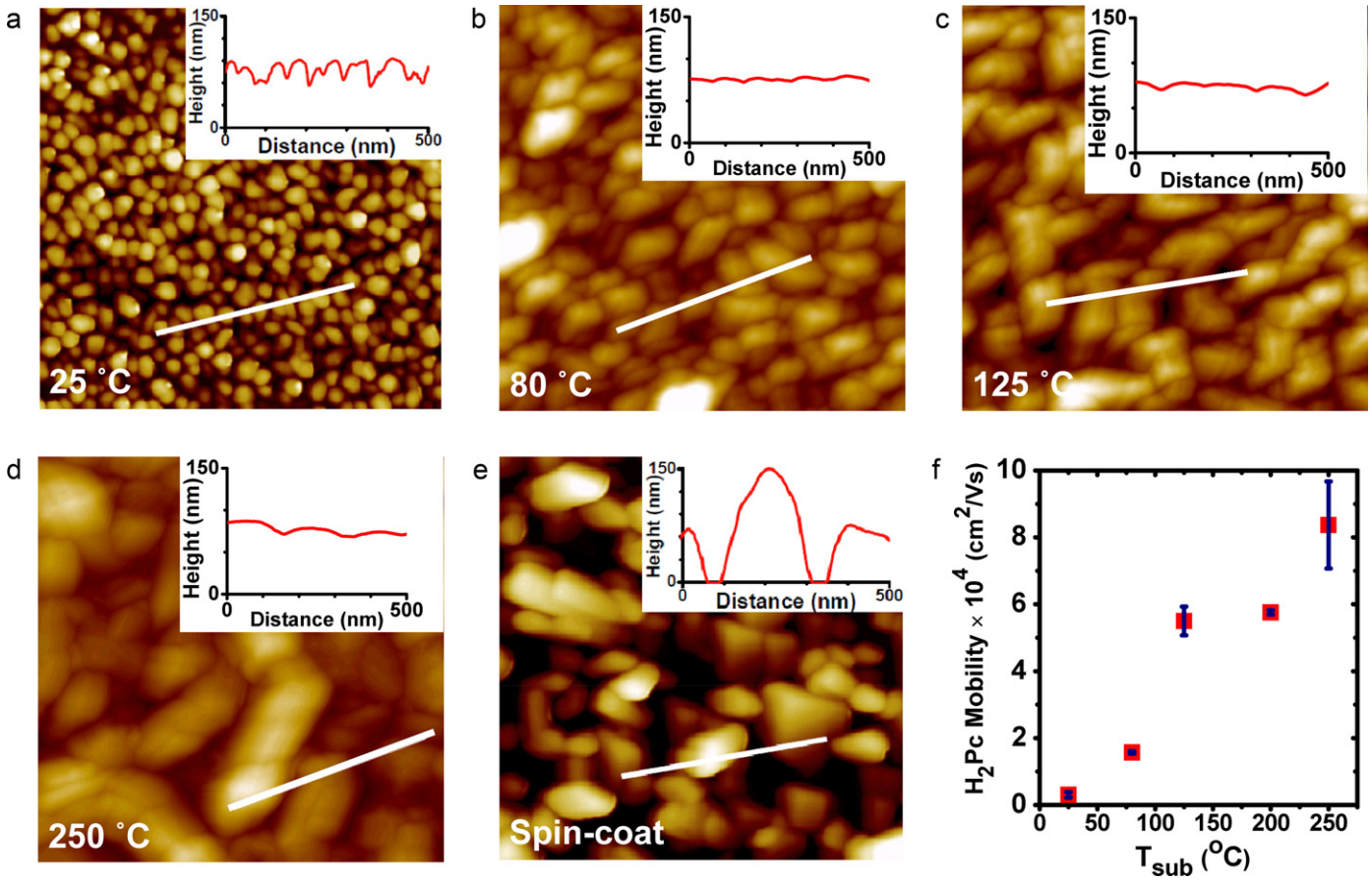

Fig. 3. H_2TBP and H_2Pc film microstructure characterization. Atomic force microscopy (AFM) images of a 1 μm × 1 μm region of 100 nm H_2Pc deposited on SiO_2 substrates held at (a) 25 °C, (b) 80 °C, (c) 125 °C, (d) 250 °C. (e) AFM image of 1 μm × 1 μm region of solution processed H_2TBP. The insets show line profiles of a 500 nm segment indicated by a white line in the image. The height scale on the line profiles is held constant to demonstrate the larger surface roughness for H_2TBP films. (f) Mobility of H_2Pc OTFTs with different substrate temperatures (T_{sub}). Some error bars are smaller than the markers.

for a small set of analytes, the data shows a significant difference between t_{60} values for strong and weak binding analytes. Strongly hydrogen-bonding analytes such as DMMP and TMP have longer recovery times and higher sensitivities; consistent with the inner N_4H_2 ring acting as the preferential binding site. This demonstrates that the different processing methods and film morphologies for H_2TBP and H_2Pc OTFTs do not significantly alter the analyte-semiconductor hydrogen-bonding characteristics that govern chemical sensing.

H_2Pc sensors show significantly shorter t_{60} for isophorone than DMMP and TMP despite having a high sensitivity to isophorone; however, anomalous recovery characteristics for isophorone in H_2Pc chemiresistors have been reported previously [29]. It has been suggested that physisorbing analytes can interact with MPc films by preferential binding or by weak van der Waals interactions with the conjugated π system of H_2TBP and H_2Pc [29]. Therefore, it is possible that the meso nitrogens present in H_2Pc, and absent in H_2TBP, contribute to sensor response and recovery. However, the fast recovery and low sensitivity for each sensor to doses of MeOH and ACN suggest that the molecular structure of the extended π system does not significantly alter sensor response.

OTFT device properties are highly dependent on fabrication methods which influence film electronic structure by affecting grain size and intermolecular coupling [43]. The different surface morphologies of 100 nm H_2Pc films with T_{sub} = 25–250 °C and a solution processed H_2TBP film are shown in atomic force microscopy (AFM) images presented in Fig. 3a–e. Line profiles of a 500 nm segment are shown as insets for each image. The height scale on the line profiles is held constant to demonstrate the larger surface roughness for H_2TBP films.

Vacuum deposited H_2Pc has a film morphology which depends on substrate temperature. At T_{sub} = 25 °C, H_2Pc forms small, densely packed grains (Fig. 3a) with an average grain size of 34 ± 12 nm and RMS roughness of 8 nm. As T_{sub} increases, the grains become large elongated crystallites with an average long-axis length of 187 ± 87 nm and aspect ratio of ~3. The large crystallite growth enhances the layer-to-layer connectivity as evidenced by a smaller RMS roughness of 5 nm. To illustrate the effect of grain size and film morphology on the H_2Pc film electronic properties, the mobility was plotted for OTFTs deposited with T_{sub} ranging from 25 °C to 250 °C (Fig. 3f). The increase in mobility with grain size is often observed for phthalocyanine OTFTs [30,44].

Following spin-coating, the bicycloporphyrin precursor forms an amorphous film with thicknesses between 100 and 200 nm. After thermal conversion to H_2TBP, large crystallites form (Fig. 3e) and create a highly textured film with average grain size of 107 ± 47 nm and root-mean-square (RMS) roughness of 28 nm. The H_2TBP OTFTs in this work have mobilities exceeding any of the H_2Pc OTFTs even though the H_2TBP films do not have the largest grain sizes. The higher mobility in H_2TBP OTFTs is consistent with enhanced intermolecular coupling and better long-range order though the H_2TBP grains.

Several reports for OTFT sensors using different molecular semiconductors note the importance of controlling grain size and surface roughness to optimize sensitivity [18,45,46]. However, the nearly identical chemical sensor response in this study suggests

that film microstructure differences do not significantly alter the H_2TBP and H_2Pc molecular interactions with analytes. The data presented are consistent with grain growth affecting the electronic delocalization and field-effect mobility of the film, but not affecting the hydrogen-bonding event that governs the relative sensor response. The data suggests that the film *inter*molecular interactions influence the mobility and are independent from the *intra*molecular interactions between the film and analyte that control chemical sensing.

4. Conclusion

In summary, OTFT sensors based on solution processed H_2TBP were found to have enhanced mobilities while yielding chemical sensing properties nearly identical to OTFT sensors based on vapor deposited H_2Pc. The mobilities of the films were strongly affected by differences in film microstructure, but this had little influence on chemical sensor behavior. This is consistent with analyte binding being chiefly a function of interactions with individual molecules of the sensor film. This study suggests the feasibility of preparing nonvolatile metal coordination complex sensor arrays with solution processed films. Consistent chemical sensor response can be obtained despite dramatic changes in field-effect mobility, which implies that relative chemical sensor response is a more robust property than field-effect mobility in OTFT sensors.

Acknowledgements

Support by AFOSR STTR II Contract Number: FA9550-10-C-0019 and NSF grant# CHE-0848502 is gratefully acknowledged. The authors would like to thank Prof. Noboru Ono at Ehime University for synthesis of the H_2TBP precursor. J.E.R. would like to thank David Martin and Erik Kappe for developing the LabVIEW programs.

Appendix A. Supplementary data

Supplementary data associated with this article can be found, in the online version, at doi:10.1016/j.snb.2011.06.030.

References

[1] L. Torsi, A. Dodabalapur, Organic thin-film transistors as plastic analytical sensors, Analytical Chemistry 77 (2005) 380A–387A.
[2] L. Torsi, G.M. Farinola, F. Marinelli, M.C. Tanese, O.H. Omar, L. Valli, F. Babudri, F. Palmisano, P.G. Zambonin, F. Naso, A sensitivity-enhanced field-effect chiral sensor, Nature Materials 7 (2008) 412–417.
[3] A.N. Sokolov, M.E. Roberts, Z.A. Bao, Fabrication of low-cost electronic biosensors, Materials Today 12 (2009) 12–20.
[4] X. Lee, Y. Sugawara, A. Ito, S. Oikawa, N. Kawasaki, Y. Kaji, R. Mitsuhashi, H. Okamoto, A. Fujiwara, K. Omote, T. Kambe, N. Ikeda, Y. Kubozono, Quantitative analysis of O-2 gas sensing characteristics of picene thin film field-effect transistors, Organic Electronics 11 (2010) 1394–1398.
[5] H.U. Khan, M.E. Roberts, O. Johnson, R. Forch, W. Knoll, Z.N. Bao, In situ, label-free DNA detection using organic transistor sensors, Advanced Materials 22 (2010) 4452–4456.
[6] H.U. Khan, J. Jang, J.J. Kim, W. Knoll, In situ antibody detection and charge discrimination using aqueous stable pentacene transistor biosensors, Journal of the American Chemical Society 133 (2011) 2170–2176.
[7] M.J. Spijkman, J.J. Brondijk, T.C.T. Geuns, E.C.P. Smits, T. Cramer, F. Zerbetto, P. Stoliar, F. Biscarini, P.W.M. Blom, D.M. de Leeuw, Dual-gate organic field-effect transistors as potentiometric sensors in aqueous solution, Advanced Functional Materials 20 (2010) 898–905.
[8] A.N. Sokolov, M.E. Roberts, O.B. Johnson, Y.D. Cao, Z.A. Bao, Induced sensitivity and selectivity in thin-film transistor sensors via calixarene layers, Advanced Materials 22 (2010) 2349–2353.
[9] K.C. See, A. Becknell, J. Miragliotta, H.E. Katz, Enhanced response of n-channel naphthalenetetracarboxylic diimide transistors to dimethyl methylphosphonate using phenolic receptors, Advanced Materials 19 (2007) 3322–3330.
[10] F. Liao, C. Chen, V. Subramanian, Organic TFTs as gas sensors for electronic nose applications, Sensors and Actuators B: Chemical 107 (2005) 849–855.
[11] J. Huang, J. Miragliotta, A. Becknell, H.E. Katz, Hydroxy-terminated organic semiconductor-based field-effect transistors for phosphonate vapor detection, Journal of the American Chemical Society 129 (2007) 9366–9376.
[12] J. Huang, T.J. Dawidczyk, B.J. Jung, J. Sun, A.F. Mason, H.E. Katz, Response diversity and dual response mechanism of organic field-effect transistors with dinitrotoluene vapor, Journal of Materials Chemistry 20 (2010) 2644–2650.
[13] M.E. Roberts, S.C.B. Mannsfeld, N. Queralto, C. Reese, J. Locklin, W. Knoll, Z.N. Bao, Water-stable organic transistors and their application in chemical and biological sensors, Proceedings of the National Academy of Sciences of the United States of America 105 (2008) 12134–12139.
[14] M.E. Roberts, S.C.B. Mannsfeld, M.L. Tang, Z.N. Bao, Influence of molecular structure and film properties on the water-stability and sensor characteristics of organic transistors, Chemistry of Materials 20 (2008) 7332–7338.
[15] G. Scarpa, A.L. Idzko, A. Yadav, E. Martin, S. Thalhammer, Toward cheap disposable sensing devices for biological assays, IEEE Transactions on Nanotechnology 9 (2010) 527–532.
[16] R.D. Yang, T. Gredig, C.N. Colesniuc, J. Park, I.K. Schuller, W.C. Trogler, A.C. Kummel, Ultrathin organic transistors for chemical sensing, Applied Physics Letters 90 (2007).
[17] T. Someya, H.E. Katz, A. Gelperin, A.J. Lovinger, A. Dodabalapur, Vapor sensing with alpha, omega-dihexylquarterthiophene field-effect transistors: the role of grain boundaries, Applied Physics Letters 81 (2002) 3079–3081.
[18] L. Torsi, A.J. Lovinger, B. Crone, T. Someya, A. Dodabalapur, H.E. Katz, A. Gelperin, Correlation between oligothiophene thin film transistor morphology and vapor responses, Journal of Physical Chemistry B 106 (2002) 12563–12568.
[19] D. Duarte, D. Sharma, B. Cobb, A. Dodabalapur, Charge transport and trapping in organic field effect transistors exposed to polar analytes, Applied Physics Letters 98 (2011).
[20] T.R.E. Simpson, D.A. Russell, I. Chambrier, M.J. Cook, A.B. Horn, S.C. Thorpe, Formation and characterization of a self-assembled phthalocyanine monolayer suitable for gas-sensing, Sensors and Actuators B: Chemical 29 (1995) 353–357.
[21] G. Guillaud, J. Simon, J.P. Germain, Metallophthalocyanines: gas sensors, resistors and field effect transistors, Coordination Chemistry Reviews 178–180 (1998) 1433–1484.
[22] T. Malinski, Z. Taha, S. Grunfeld, A. Burewicz, P. Tomboulian, F. Kiechle, Measurements of nitric-oxide in biological-materials using a porphyrinic microsensor, Analytica Chimica Acta 279 (1993) 135–140.
[23] N.R. Armstrong, Phthalocyanines and porphyrins as materials, Journal of Porphyrins and Phthalocyanines 4 (2000) 414–417.
[24] M. Bora, D. Schut, M.A. Baldo, Combinatorial detection of volatile organic compounds using metal-phthalocyanine field effect transistors, Analytical Chemistry 79 (2007) 3298–3303.
[25] F.I. Bohrer, C.N. Colesniuc, J. Park, I.K. Schuller, A.C. Kummel, W.C. Trogler, Selective detection of vapor phase hydrogen peroxide with phthalocyanine chemiresistors, Journal of the American Chemical Society 130 (2008) 3712.
[26] N.A. Rakow, A. Sen, M.C. Janzen, J.B. Ponder, K.S. Suslick, Molecular recognition and discrimination of amines with a colorimetric array, Angewandte Chemie-International Edition 44 (2005) 4528–4532.
[27] B. Wang, X. Zuo, Y.Q. Wu, Z.M. Chen, C.Y. He, W.B. Duan, Comparative gas sensing in copper porphyrin and copper phthalocyanine spin-coating films, Sensors and Actuators B: Chemical 152 (2011) 191–195.
[28] F.I. Bohrer, A. Sharoni, C. Colesniuc, J. Park, I.K. Schuller, A.C. Kummel, W.C. Trogler, Gas sensing mechanism in chemiresistive cobalt and metal-free phthalocyanine thin films, Journal of the American Chemical Society 129 (2007) 5640–5646.
[29] F.I. Bohrer, C.N. Colesniuc, J. Park, M.E. Ruidiaz, I.K. Schuller, A.C. Kummel, W.C. Trogler, Comparative gas sensing in cobalt, nickel, copper, zinc, and metal-free phthalocyanine chemiresistors, Journal of the American Chemical Society 131 (2009) 478–485.
[30] Z.N Bao, A.J. Lovinger, A. Dodabalapur, Highly ordered vacuum-deposited thin films of metallophthalocyanines and their applications in field-effect transistors, Advanced Materials 9 (1997) 42.
[31] P.B. Shea, C. Chen, J. Kanicki, L.R. Pattison, P. Petroff, H. Yamada, N. Ono, Polycrystalline tetrabenzoporphyrin organic field-effect transistors with nanostructured channels, Applied Physics Letters 90 (2007).
[32] P.B. Shea, J. Kanicki, Y. Cao, N. Ono, Methanofullerene-coated tetrabenzoporphyrin organic field-effect transistors, Applied Physics Letters 87 (2005).
[33] J. Park, R.D. Yang, C.N. Colesniuc, A. Sharoni, S. Jin, I.K. Schuller, W.C. Trogler, A.C. Kummel, Bilayer processing for an enhanced organic-electrode contact in ultrathin bottom contact organic transistors, Applied Physics Letters 92 (2008).
[34] J.E. Royer, J. Park, C. Colesniuc, J.S. Lee, T. Gredig, S. Lee, S. Jin, I.K. Schuller, W.C. Trogler, A.C. Kummel, Mobility saturation in tapered edge bottom contact copper phthalocyanine thin film transistors, Journal of Vacuum Science & Technology B 28 (2010), C5F22–C5F27.
[35] S. Ito, T. Murashima, H. Uno, N. Ono, A new synthesis of benzoporphyrins using 4, 7-dihydro-4,7-ethano-2H-isoindole as a synthon of isoindole, Chemical Communications (1998) 1661–1662.
[36] P.B. Shea, J. Kanicki, N. Ono, Field-effect mobility of polycrystalline tetrabenzoporphyrin thin-film transistors, Journal of Applied Physics 98 (2005).
[37] P.B. Shea, A.R. Johnson, N. Ono, J. Kanicki, Electrical properties of staggered electrode, solution-processed, polycrystalline tetrabenzoporphyrin field-effect transistors, IEEE Transactions on Electron Devices 52 (2005) 1497–1503.
[38] L. Torsi, F. Marinelli, M.D. Angione, A. Dell'Aquila, N. Cioffi, E. De Giglio, L. Sabbatini, Contact effects in organic thin-film transistor sensors, Organic Electronics 10 (2009) 233–239.
[39] A. Salleo, R.A. Street, Light-induced bias stress reversal in polyfluorene thin-film transistors, Journal of Applied Physics 94 (2003) 471–479.

[40] R.D. Yang, J. Park, C.N. Colesniuc, I.K. Schuller, W.C. Trogler, A.C. Kummel, Ultralow drift in organic thin-film transistor chemical sensors by pulsed gating, Journal of Applied Physics 102 (2007).
[41] C. Laurence, J. Graton, M. Berthelot, F. Besseau, J.Y. Le Questel, M. Lucon, C. Ouvrard, A. Planchat, E. Renault, An enthalpic scale of hydrogen-bond basicity. 4. Carbon pi bases, oxygen bases, and miscellaneous second-row third-row, and fourth-row bases and a survey of the 4-fluorophenol affinity scale, Journal of Organic Chemistry 75 (2010) 4105–4123.
[42] R.D. Yang, J. Park, C.N. Colesniuc, I.K. Schuller, J.E. Royer, W.C. Trogler, A.C. Kummel, Analyte chemisorption and sensing on n- and p-channel copper phthalocyanine thin-film transistors, Journal of Chemical Physics 130 (2009).
[43] D.J. Gundlach, J.E. Royer, S.K. Park, S. Subramanian, O.D. Jurchescu, B.H. Hamadani, A.J. Moad, R.J. Kline, L.C. Teague, O. Kirillov, C.A. Richter, J.G. Kushmerick, L.J. Richter, S.R. Parkin, T.N. Jackson, J.E. Anthony, Contact-induced crystallinity for high-performance soluble acene-based transistors and circuits, Nature Materials 7 (2008) 216–221.
[44] D.G. de Oteyza, E. Barrena, J.O. Osso, H. Dosch, S. Meyer, J. Pflaum, Controlled enhancement of the electron field-effect mobility of F16CuPc thin-film transistors by use of functionalized SiO_2 substrates, Applied Physics Letters 87 (2005).
[45] L. Wang, D. Fine, A. Dodabalapur, Nanoscale chemical sensor based on organic thin-film transistors, Applied Physics Letters 85 (2004) 6386–6388.
[46] J. Park, J.E. Royer, C.N. Colesniuc, F.I. Bohrer, A. Sharoni, S.H. Jin, I.K. Schuller, W.C. Trogler, A.C. Kummel, Ambient induced degradation and chemically activated recovery in copper phthalocyanine thin film transistors, Journal of Applied Physics 106 (2009).

Biographies

James Royer received his B.S. degree in chemistry from the University of Maryland, College Park and is a Ph.D. candidate in chemistry at the University of California, San Diego. His current research interests include chemical sensing in organic thin film transistors and molecular adsorption on organic monolayers studied by scanning tunneling microscopy.

Sangyeob Lee received his B.S. in ceramic engineering from Kyungpook National University in 2003, and received his M.S. (in 2004) from University of Southern California and Ph.D. (in 2009) from University of California, Irvine, both in materials science. He is currently a post-doctoral researcher at the University of California, San Diego. His research interests include chemical sensing in organic thin film transistors and scanning probe microscopy on organic materials.

Charlene Chen received the B.S. degree in electrical engineering from the National Taiwan University, Taipei, Taiwan, in 2005 and the M.S. degree in electrical engineering from the University of Michigan, Ann Arbor, in 2006, where she is currently working toward the Ph.D. degree at the Department of Electrical Engineering and Computer Science, under the supervision of Prof. Kanicki. Her current research mainly focuses on a-InGaZnO TFTs and their application to active-matrix organic light-emitting displays.

Byungmin Ahn received a Ph.D. degree from the University of Southern California (USC) in 2008. He is currently a postdoctoral research associate at USC. His research interests include mechanical metallurgy and electron microscopy.

Jerzy Kanicki received the Ph.D. degree in sciences from the Free University of Brussel, Brussels, Belgium, in 1982. He subsequently joined the IBM Thomas J. Watson Research Center, Yorktown Heights, NY, as a Research Staff Member working on hydrogenated amorphous silicon devices for photovoltaic and flat panel display applications. In 1994, he moved to the University of Michigan where he did leading work on various flat panel display technologies and on a variety of fundamental problems related to organic and molecular electronics. He is the author and coauthor of over 250 publications in journals and conference proceedings.

William Trogler graduated from Johns Hopkins University in 1974, obtaining both and M.A. and B.A. degrees in chemistry before moving to Caltech for his Ph.D. with Harry Gray. In recent years, his research interests have centered on luminescent polymer sensors for explosives, thin film resistive chemical vapor sensors, and biomedical applications of nanoparticles. He is the author of over 180 papers.

Andrew Kummel graduated from Yale University in 1981 with a B.S. in chemical engineering. He received an M.S. degree in chemical engineering and Ph.D. in chemistry from Stanford University in 1988. Since 1996 he has been full professor of chemistry and biochemistry and an affiliated faculty member in materials science, nanoengineering, and electrical engineering. He is the author of over 120 papers. His current research interests include (a) atomic and electronic structure of oxide–semiconductor interfaces using STM/STS probes; (b) chemically sensitive field effect transistor sensing; and (c) nanoshell and microshell based drug delivery, drug detection, and cancer detection.